Developing high performance RF heating scenarios on the WEST tokamak

M.Goniche[1], V.Ostuni[1], C.Bourdelle[1], P.Maget[1], J.F.Artaud[1], J.M.Bernard[1], V.Bobkov[2], J.Bucalossi[1], F.Clairet[1], L.Colas[1], C.Desgranges[1], L.Delpech[1], P.Devynck[1], R.Dumont[1], A.Ekedahl[1] N.Fedorczak[1], J.Garcia[1], J.Gaspar[3], C.Gil[1], C.Guillemaut[1], J.Gunn[1], J.Hillairet[1], C.Klepper[4], C.Lau[4], E.Lerche[5], G.Lombard[1], P.Manas[1], E.H.Martin[4], D.Mazon[1], O.Meyer[1], J.Morales[1], Ph.Moreau[1], E.Nardon[1], R.Nouailletas[1], B.Pegourié[1], M.Peret[1], Y.Peysson[1], X. Regal-Mezin[1], R.Sabot[1], S.Shiraiwa[6], G.Urbanczyk[1], L.Vermare[7], D.Vezinet[1], G.M.Wallace[8] and the WEST Team*

[1] CEA, IRFM, F-13108 Saint Paul-lez-Durance, France

[2] Max-Planck Institut für plasmaphysik, Boltzmannstraße 2, 85748 Garching, Germany

[3] Aix Marseille Université, CNRS, IUSTI, Marseille, France

[4] Oak Ridge National Laboratory, Oak Ridge, Tennessee 37831-6169, USA

[5] Laboratory for Plasma Physics, Royal Military Academy, 1000 Bruxelles, Belgium

[6] Princeton Plasma Physics Laboratory, Princeton, USA

[7] Ecole Polytechnique, LPP, CNRS UMR 7648, 91128 Palaiseau cedex. France

[8] MIT Plasma Science and Fusion Center, Cambridge, MA 02139, USA

*http://west.cea.fr/WESTteam

e-mail marc.goniche@cea.fr

Abstract

High power experiments, up to 9.2 MW with LHCD and ICRH, have been carried out in the full tungsten tokamak WEST. Quasi non inductive discharges have been achieved allowing to extend the plasma duration to 53s with stationary conditions in particular with respect to tungsten contamination. Transitions in H mode are obtained lasting up to 4s with weak energy increment at the power crossing the separatrix is close to the threshold. Hot L mode plasmas ($T_e(0)$>3keV) with a confinement time following the ITER L96 scaling are routinely obtained. The weak aspect ratio dependence of this scaling law is confirmed. Tungsten accumulation is generally not an operational issue on WEST. Difficulty of burning through tungsten can prevent from accessing to a hot core plasma in the ramp-up phase or can lead to rapid collapse of the central temperature when radiation is enhanced by a slight decrease of the temperature. Apart few pulses post-boronization, the plasma radiation is rather high (P_{rad}/P_{tot}~50%) and is dominated by tungsten. This fraction does not vary as the RF power is ramped up and is quite similar in ICRH and/or LHCD heated plasmas. An estimate of the contribution of the RF antennas to the plasma contamination in tungsten is given.

1. Introduction

In a tungsten environment, development of high power scenarios is often undermined by inward transport of tungsten (W) in the very core of the plasma leading to a loss of energy confinement [1, 2]. WEST, a medium size (R=2.5m, a=0.45m) actively cooled full W tokamak aiming at power exhaust studies in long / steady-state pulses, is addressing this issue with RF only heating and current drive systems.

WEST can operate in lower single null (LSN), upper single null (USN) and double null configurations with an aspect ratio ranging between 5 and 6. The lower divertor was partially made of actively cooled ITER-like target completed by inertial W coated plasma facing units in phase 1 (2017-2021) and it will be fully made of ITER-like plasma-facing components (PFCs) in phase 2 starting in 2022 [3, 8]. Two lower hybrid current drive (LHCD) launchers (LH1 and

LH2) and three ion cyclotron resonance heating (ICRH) antennas (IC1, IC2 and IC3) have been installed and commissioned. All antennas are actively-cooled and equipped by tungsten-coated guard limiters.
In the 2018 and 2019 campaigns, once a reliable start-up of the plasma could be found [4, 5], the LHCD and ICRH coupled powers have both reached ~5MW/1s separately (up to 5.3MW/4s for LHCD) and 9MW/0.5s when combining the two RF systems [6, 7, 8]. The heat fluxes on the divertor outer strike point region is about 6 MW m^{-2} with a total injected power of 4 MW of LHCD power with a radiated fraction in a range of 50%. These results are very encouraging and they exhibit the capability to reach 10 MW m^{-2} with about 7 MW of additional power in L-mode plasma [9].
The experiments were performed at high magnetic field (B_t=3.6-3.7T) in a large range of plasma configurations: X-point plasmas (R~2.5m, a~0.45m, κ~1.3) in LSN and USN configuration, plasma current in the 0.3-0.7MA range (q_{95}~3-6) and line-averaged electron density in the 2.5-8.5×$10^{19}m^{-3}$ range (n_e/n_{GW}=0.3-0.8).
The paper is organized as follows: the scaling of the stored energy and energy confinement of the entire database is first established. H-mode access is also presented in this section. Section 3 shows the interplay between the electron heating and the bulk radiation. Results addressing the LHCD efficiency in view of long pulse operation are shown in section 4. Bulk plasma radiation and W content of LH, IC and LH+IC discharges are presented in section 5. The temperature collapse observed on many discharges is discussed in section 6. Estimates of the contribution of the RF antennas to the plasma contamination are given in section 7.
The density n_e is the line-averaged density unless otherwise specified. The confined plasma will be mentioned as 'bulk plasma' and the central part of the plasma as 'core plasma'. LHCD antennas are named LH1and LH2 and the ICRH antennas IC1, IC2 and IC3.IC2 is the closest antenna to the LHCD ones. Data are, unless specified, averaged on a one-second time window.

2. Energy confinement and H-mode access

2.1. Scaling of the energy confinement time of the L-mode discharges

The energy confinement of the L-mode discharges is compared with the ITER L mode scaling law ITER96L [10]. WEST has a larger aspect ratio than most tokamaks that have contributed to this scaling law, as illustrated by figure 1.

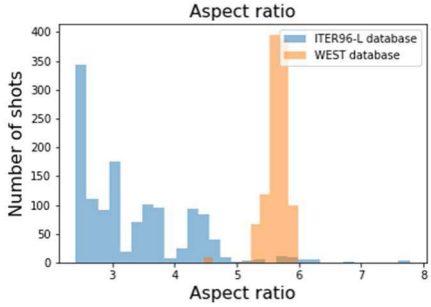

Figure 1; Number of pulses in the ITER L mode database against the aspect ratio

The parametric dependence of the confinement time with respect to the aspect ratio (A) is obtained by adding WEST data to the existing ITER database with machines having A ranging from 2.41 to 7.78, but with few shots in the range 5-6 [10]. WEST database contains more than 1000 entries in L mode (I_p=0.2-0.8MA, P_{AUX}=0.5-9MW, n_e= 1-9 $10^{19}m^{-3}$), deuterium only pulses, heated by LHCD and/or ICRH with 80% of the data points from discharges with LHCD only. The performed studies take into account statistics calculated on plateaus of total power intersecting plasma current plateaus whose duration exceeds 0.5s (quasi-steady states).

The plasma energy content W_{MHD} computed from polarimetry and magnetics constrained equilibrium reconstructions using NICE [11] is chosen for the analysis and only the reconstructions having the electron density interfero-polarimetry line-integrated measurements which differ from that obtained by the equilibrium code by less than 20% are kept. The contribution of the IC fast ions energy to W_{MHD} is expected to be small for density n_e> 4 $10^{19}m^{-3}$, lower than 10%. Only discharges in deuterium and LSN are considered.

The energy confinement time is defined as the ratio between the total energy content (W_{MHD}) and the total heating power corrected for $\frac{dW_{MHD}}{dt}$.

The engineering parameters scaling law is:

$$\tau = C\, I_P^{\alpha_{I_P}} n_e^{\alpha_n} P_{tot}^{\alpha_P} A^{\alpha_A} B^{\alpha_B} k^{\alpha_k} R^{\alpha_R} M^{\alpha_M}$$

where I_P is the total plasma current in MA, n_e is the line averaged electron density in 10^{19}m^{-3}, P_{tot} is the total power in MW, A is the aspect ratio, B is the toroidal magnetic field in T, k is the plasma elongation, R the major radius in m and M is the isotope mass.

The scaling law of the confinement time can also be established with dimensionless parameters [12]:

$$\Omega_i \tau = \rho_*^{x_{\rho_*}} \beta^{x_\beta} \nu_*^{x_{\nu_*}} q^{x_q} M^{x_M} \varepsilon^{x_\varepsilon} B^{x_B} k^{x_k} \text{ accounting for the Kadomtsev constraint } x_B = 0$$

where ρ_* is the ratio of the Larmor radius to the tokamak minor radius, β is the ratio of the kinetic and magnetic pressures, ν_* is the collision frequency normalized to the transit time frequency, q is the safety factor, ε is the inverse aspect ratio.

Since A, B, k, R and M are fixed, the WEST scaling is derived with respect to the plasma current, line averaged electron density and total power (first line of table 1). The WEST discharges have a stronger plasma current dependency and an unfavorable effect of the density on the confinement with respect of the ITER-L scaling law (line 2 of table 1). On JET, in H-mode, higher I_p and lower n_e exponents were found with the metallic wall when compared to the previous JET configuration with the carbon wall, like the ITER 96-L database [13]. The density scaling might also be due to the modified LHCD absorption as the density increases and is discussed later. When the ITER96-L mode scaling law is applied to WEST data, the RMSE between predicted energy content and measured is 21%, while it is reduced to 12.7% when adjusting the scaling factors to the WEST database.

WEST data are added to the existing ITER96-L mode database. It contains 1312 entries coming from 12 different tokamaks. It is important to remind that only the τ_{mhd} is available for WEST data, while the one used for ITER96-L database is the thermal energy confinement time. It is assumed that τ_{mhd} is close to τ_{th} in WEST.
It is important to note that in the ITER96-L database the radiated power has not been subtracted from the total power as this is a small fraction of the total power. For WEST, this assumption is not valid, as the radiated power in the core is high due to the rather large density of tungsten but the fraction of the input power which is radiated is weakly sensitive to the power and density as it will be detailed in section 5. When the radiated power is subtracted to the input power the coefficients are weakly affected as shown in the appendix and the total input power can be used for establishing the scaling.
Moreover, a generalized linear model regression is used in order to take into account the Kadomtsev constraint $\chi_B = 0$ [14]:

$$\chi_B = \frac{5 + 5\alpha_B - 4\alpha_R + \alpha_{I_p} + 3\alpha_P + 8\alpha_{n_e}}{5(1 + \alpha_P)}$$

The results of both dimensional and dimensionless scaling laws are reported in lines 3 and 5 of table 1. Even if WEST has an aspect ratio larger than the other tokamaks in ITER96-L database, the regression coefficient for the aspect ratio is still close to zero, this means that it does not play an important role in the scaling. Although the WEST shots are well aligned with the ITER96-L mode database, there are some important differences when comparing the exponents of the dimensionless parameters. The uncertainty on these parameters is intrinsically larger than that on the dimensional parameters [12]. When the Kadomtsev transformation is used, α_P appears as denominator in each coefficients transformation formula and a weak variation of α_P leads to a big change in the dimensionless coefficients.

Table 1 – Coefficients of the dimensional and dimensionless scaling laws for WEST database (line 1), ITER database (line 2 and 4 and WEST database merged with ITER database (line 3 and 5).

	I_p	n_e	P_{tot}	A	B_T	k	R	M_{eff}	Ent.
τ_{mhd} WEST scaling	1.30	-0.20	-0.73	-	-	-	-	-	1083
τ_{th} ITER-L scaling	0.96	0.40	-0.73	0.06	0.03	0.64	1.83	0.20	1313

ITER + WEST data	1.06	0.23	-0.73	0.15	0.09	0.53	1.55	0.19	2396
	q	B_T	k	A	M_{eff}	ρ_*	ν_*	β	Ent.
τ_{th} ITER-L scaling	-3.74	0	3.22	0.04	0.67	-1.85	-0.19	-1.41	1313
ITER +. WEST data	-4.30	0	3.67	0.01	0.73	-1.62	-0.09	-2.18	2396

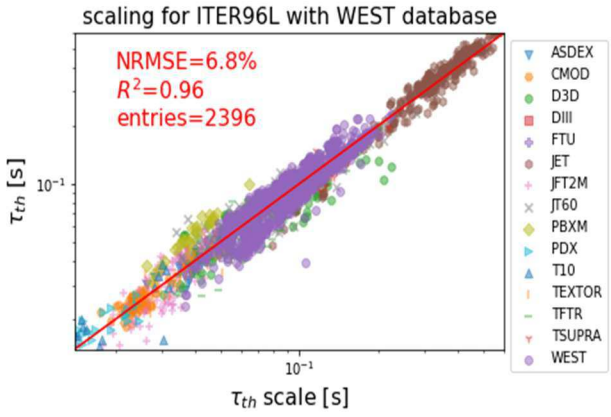

Figure 2. Energy confinement time, derived from the equilibrium reconstructions W_{MHD}, for the existing ITER-L96 database merged with 1087 WEST additional entries (see table 1).

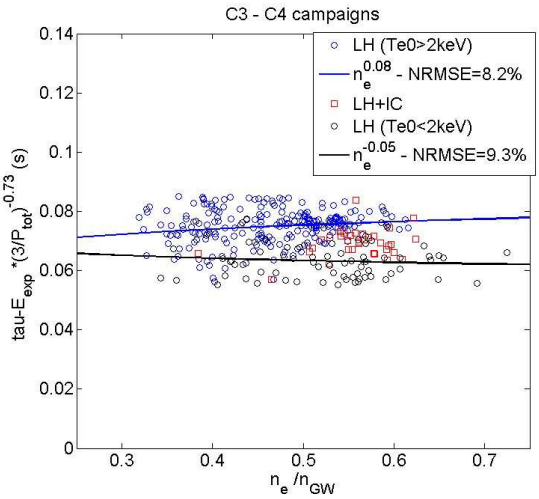

Figure 3. Energy confinement time versus line average density normalized to the Greenwald density for LHCD only (circles) and LHCD+ICRH (squares) discharges (B_t=3.7T, Ip=0.5MA) The confinement time has been rescaled for P_{tot}=3MW assuming a $P^{-0.73}$ scaling. The solid lines are best fits for the LHCD discharges. Only discharges with LH/IC power exceeding 0.8MW are considered.

2.2. Scaling of the confinement with density for two heating schemes

The scaling of the confinement with density of the LHCD only discharges is compared to that of LHCD+ICRH discharge performed with I_p=0.5MA. This was done on a more limited number of entries, each entry being the stored energy, W_{MHD}, of a discharge averaged over one second. As discussed in section 4, the core temperature of many WEST discharges (~30%) does not increase above 1.8keV when the power is ramped up. The discharges with low and high central electron temperature Te0 have been grouped in two sets. The confinement time is rescaled for a power of 3MW taking into account the WEST power scaling $P^{-0.73}$(Table 1). The discharges combining the two heating systems have a lower confinement time by 10% on average compared to the high Te0 group of LH only discharges (Figure 3). This is mainly understood as the result of poor electron heating provided by the IC waves as discussed in section 4.

The confinement of the LHCD discharges with high Te0 is almost insensitive to the plasma density ($\tau_E \sim n_e^{0.08}$) up to $n_e \sim 4.5\times10^{19} m^{-3}$ (n_e/n_{GW}=0.57) when the ITER-L scaling and the Tore Supra scaling (also established for LHCD discharges [15]) has a quite strong dependence ($\tau_E \sim n_e^{0.4}$). At higher densities, the normalized confinement time seems to level off and would be very likely the result of lower current drive efficiency leading to lower electron heating after slowing down of the fast electrons. Experiments performed at higher densities, up to n_e/n_{GW}=0.7, would be necessary to confirm. Possible reduction of current drive efficiency at high density is discussed in section 3.

2.3. L-mode to H-mode transition

L-H transition was observed, after fresh boronization, when combining 4MW of LHCD with 1MW of ICRH (Figure 4), both in LSN where the $\vec{B} \times \vec{\nabla} B$ is directed towards the X point, in the so-called favorable configuration, as well as in the USN, so-called unfavorable configuration [12]. They occur for power crossing the separatrix slightly below the Martin 2008 scaling law and at densities below the minimum in density predicted by Ryter scaling [19], as illustrated in figure 5. Therefore, the ELM free transitions observed so far in WEST are likely transitions occurring on the low density branch [20]. It results a significant increase of the particle confinement time (30% increase of plasma density with gas injection turned off). In LSN, a pedestal is observed on the density profiles measured by reflectometry concomitant with a clear and deep deep radial electric field (Er) well just inside the separatrix observed on the velocity profile measured by Doppler Back scattering. Deeper Er wells are observed in USN configuration during similar transitions with less pronounced density pedestal [12]. A signature of the pedestal is also seen on the internal inductance which decreases from 0.85 to 0.75 (figure 5) while the current driven by the LH waves does not flatten (the peaking of the HXR profile is unchanged), indicating a flattening of the total current profile caused by a higher bootstrap current at the edge. Nonetheless, the stored energy increases by only 5-10% (figure 5). The increment in total energy content thanks to the pedestal is weakened by a reduction of the core electron temperature (figure 5) at the transition concomitant with an increment in the radiated power (figure 5). Such increment of the radiated power following the transition and leading to weak H mode phases are also reported in JET at low density in deuterium [20] and in tritium [21].

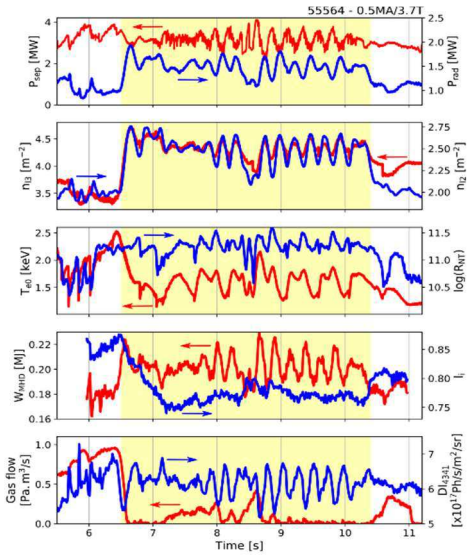

Figure 4. 4-second H-mode discharge in LSN configuration. Total power P_{tot} is the combination of 4MW of LHCD with 1MW of ICRH.

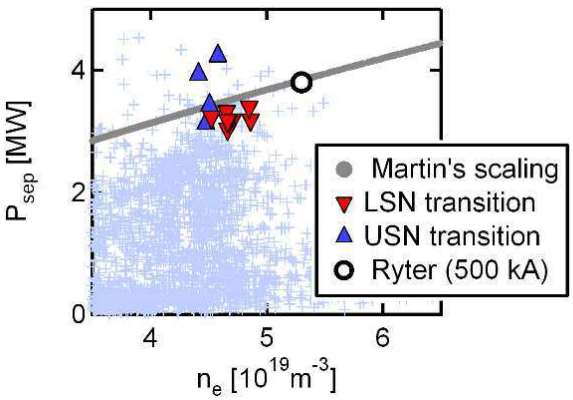

Figure 5. P_{sep} versus density for the whole C4 campaign. The grey line is the Martin's scaling for L-H transition.

3. Lower hybrid current drive and long pulse operation

In low loop voltage discharges (V_L<0.1V), the LHCD efficiency can be estimated with an accuracy of ±10% from the loop voltage in the ohmic heating (OH) phase, the ratio of the plasma resistivity ρ_{LH}/ρ_{OH} and the faction of bootstrap current I_{BS}/I_p [22]. This LHCD efficiency η is found to be 0.7-0.8×10^{19} A.W^{-1}.m^{-2} for the best discharges (Figure 6). The discharge with a dithering H-mode is one of these discharges. This current drive efficiency is in line with that observed on Tore Supra for limiter discharges at higher plasma current but quite similar safety factor (q_{95}=4-5).. Remarkably, the discharge at the lowest density (2.9×$10^{19}$$m^{-3}$) with high temperature (Te0~6keV) has a similar LHCD efficiency as the high density (4.2×$10^{19}$$m^{-3}$) H-mode discharge with much lower temperature (Te0=3.7keV). For these two discharges, the bremsstrahlung profiles, derived from the 33 lines-of-sight of the hard X-ray (HXR) diagnostic, are very similar with same amplitude but very slightly broader profile for the low density case (figure 7). However

the high density case has a higher W density in the core by a factor ~1.5 and the bremsstrahlung caused by the collisions of the fast electrons with the partially ionized tungsten atoms can strongly increase the HXR signals. It can result a decoupling between the LH current profile and the HXR profile [23].

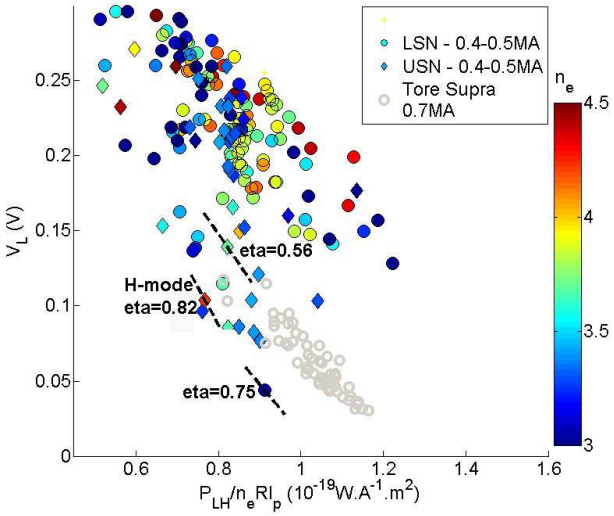

Figure 6. Loop voltage as a function of normalized LHCD power. The LHCD efficiency eta (unit: 10^{19} $A.W^{-1}.m^{-2}$) is shown for 3 discharges.

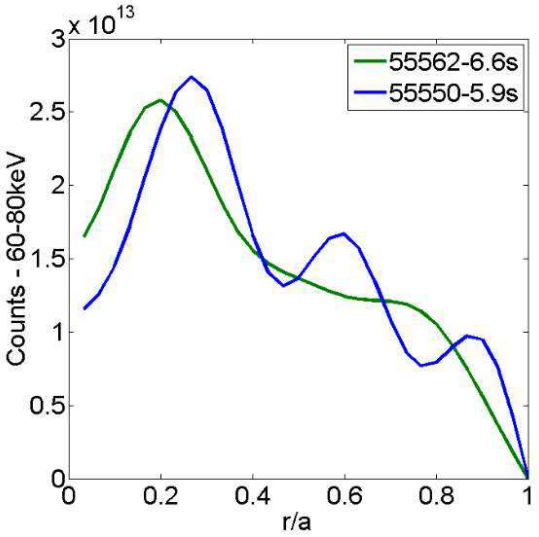

Figure 7. HXR profiles of the low density discharge (#55550) and the high density H-mode discharge (#55562).

The polarization of the lower hybrid wave was inferred from a visible spectroscopy diagnostic measuring the D_β spectral line profiles, 3-6 centimeters in front of the launcher [24]. At low density (n_e <$4x10^{19}m^{-3}$), the polarization is found to be as expected for the slow wave but at higher density, a significant rotation of the polarization is measured on some discharges, leading to a poloidal component which can be as high as the radial component. In that case, less power is available for central absorption and current drive efficiency, when calculated with the total launched LH power, is degraded, as observed on Alcator C-Mod [25] and suggested by the density scaling of the confinement time (see table 1).

A loop voltage of ~100mV allows on WEST at medium density (n_e=3.3-3.7×$10^{19}m^{-3}$) extending the discharge duration to 53 seconds. This duration was not limited by magnetic flux consumption but by the temperature of the central solenoid (Figure 8). All plasma parameters are steady in particular the total radiation and the density of highly ionized W atoms (W^{43+}) representative of the W content in the core of the discharge as the variation of the electron temperature and density does not exceed 10%.

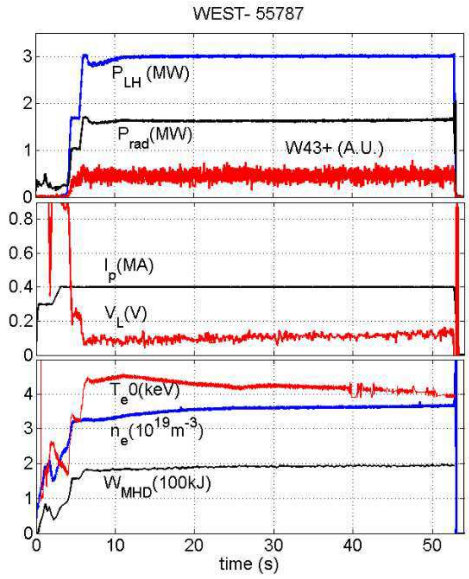

Figure 8. 53-second discharge (Bt/Ip=3.7T/0.4MA, USN configuration).

4. Electron heating with LHCD and ICRH

Lower hybrid waves tailored for current drive (wave parallel index N//=1.9 for these experiments) and ion cyclotron waves in the minority heating scheme (hydrogen minority concentration estimated to be in the range of 5-10%) predominantly heat the electrons, respectively, by slowing down of the fast electrons and collisional power redistribution of the fast ions. When the central electron temperature Te0 is plotted as a function of the total power normalized to the line-averaged density P_{tot}/n_e, two regimes with different ranges of Te0 are clearly seen (Figure 9). There is, first, a regime where the temperature increases with P_{tot}/n_e and Te0 exceeds 3keV when $P_{tot}/n_e > 0.8$-1 (circles of figure 9). These discharges have high internal inductance and good global energy confinement whereas for the other discharges, the temperature does not increase beyond 2keV (squares of figure 9).

In the first case, the observed saturation of Te0 of these discharges, mostly combining ICRH and LHCD at higher density, is caused either by reduction of electron heating with LHCD (see section 2) or poor electron heating with ICRH, as discussed later in this section.-These two regimes reflect the difficulty of burning-through W. The W cooling factor has a negative slope between 1.5 and 3 keV. It results that any source of Te reduction (increase of density for example) will increase the core W radiation (at constant W source) which will decrease further the core temperature leading to unstable plasma radiation conditions until the core Te reaches 1.5keV above which the cooling factor is quasi Te-independent.

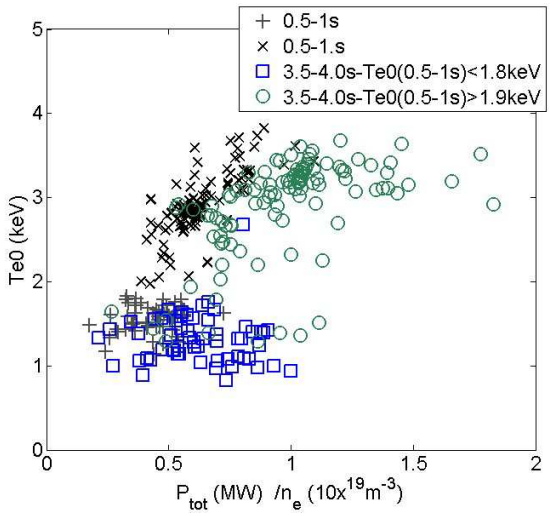

Figure 9. Central electron temperature Te0 as a function of P_{tot}/n_e 3.5-4s (circles, squares) and 0.5-1s (+, ×) after the start of the RF power (Bt=3.7T, Ip=0.5MA)

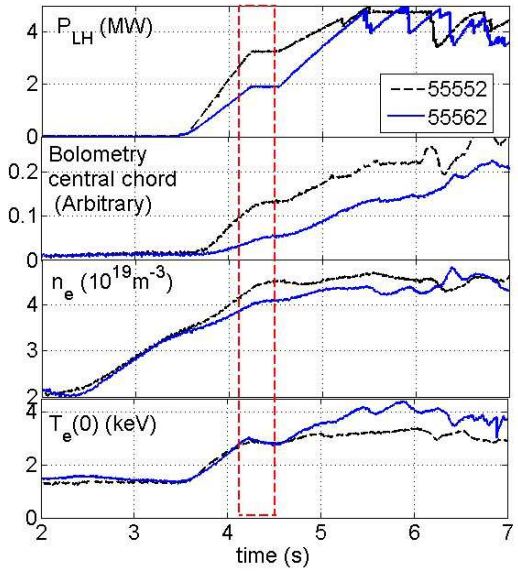

Figure 10. Two discharges with high density in the power ramp-up. The red broken line indicates the time window when P_{tot}/n_e is considered in the ramp-up phase.

The two temperature branches appear very soon during or after the ramp-up phase of power and density. When Te0 exceeds 1.9keV ~0.75s after the start of the power ramp (× symbols of figure 9), 4 discharges out of 67 have a temperature below 2 keV, 4 seconds after the start of the high power. Conversely only one discharge with low temperature in the early phase (+ symbols of figure 9), out of 59, accesses the high confinement regime. Significant correlation is also found between the temperature in the ohmic heating phase and the temperature in stationary phase, although not as good as the one with the temperature in the early RF power phase. When the initial temperature in the ohmic phase exceeds 1.5keV (resp. 1.3keV), all (respectively 85% of) the discharges have high confinement in the density and power plateau phase.

Although most of the discharges with initial temperature greater than 1.5keV were performed without nitrogen gas injection during the current ramp-up, this low-Z impurity was found efficient to increase the temperature of the ohmic heating phase. It results in an increase of the plasma resistivity in the peripheral region that leads to faster current diffusion and a strong peaking of the temperature with a central temperature increasing from ~1keV to ~2keV [26].

Fast ramp of P_{tot}/n_e gives access to high temperature in most cases, as shown on figure 9 (× symbols) and most of the low temperature branch discharges (+ symbols) suffer from a too low value of this parameter. However a significant fraction (27%) of the low confinement discharges has P_{tot}/n_e exceeding 0.5 at t~0.75s after the start of the power ramp. Although P_{tot}/n_e is ramped at the same rate for these discharges, the density is ramped too fast (or the density is too high before the power ramp) compared to the discharges with high electron temperature. When the density at this time does not exceed $3.3\times10^{19}m^{-3}$ with P_{tot}/n_e >0.5, 95% of the discharges access the high temperature branch of figure 9. For easing the wave coupling, it can be necessary to ramp the density faster. When the normalized power is pushed to P_{tot}/n_e=0.74 (figure 10, broken line), the density at the same time can be as high as $4.35\times10^{19}m^{-3}$. When the tungsten contamination is weak (after a boronization), high density ($n_e=4.0\times10^{19}m^{-3}$) and relatively low power (P_{tot}/n_e=0.49) lead to high core temperature on the plateau (figure 10, solid line).

The saturation of Te0 at high P_{tot}/n_e for discharges combining LHCD and ICRH (figure 9) indicates that modest electron heating is provided by the IC waves or electron heating is less efficient with LHCD at high density. The same trend is also observed for the energy confinement (see section 2). For the discharge shown in figure 11, weak electron heating with ICRH is observed when comparing the LHCD-only phase (3MW) to the LHCD+ICRH (2+3MW) phase. When 3MW of ICRH is coupled to a plasma pre-heated with LHCD, the incremental bulk radiation is low ($\Delta P_{rad-Bulk}/P_{ICRH}$ ~35%) and the core plasma radiation (r/a<0.2) normalized to the total power ($P_{LH}+P_{IC}$=2+3MW) is reduced

by 25% when compared to the LH phase (P_{LH}=3MW). However the central electron temperature is lower in the combined heating phase. From METIS interpretative modelling [27] based on ECE fits for Te and interferometry inversion for the density profiles, the electron stored energy is also lower but the ratio of the energy stored by the ions (inferred from DD neutron rate) increases from 35% to 45% of the total energy content. Large amplitude sawteeth indicate the presence of a fast ion population within the q=1 surface. These sawteeth do not cause a modulation of the core W density as observed at higher plasma current when the q=1 surface is broader. It should be noted that the LHCD+ICRH phase has a slighly more peaked T_e profile although density is slightly higher (~+10%) compared to the LHCD-only phase. Modelling of LHCD by a reduced model included in METIS and ICRH by the full wave code EVE [28] confirms more central, but also broader, power deposition for the phase combining the two RF heating systems). Inside the r/a=0.2 surface, the mean heating power increases by at least a factor two when the radiated power increases by less than 50% (figure 12) and discards the detrimental effect of core radiation on electron heating. Finite orbit width effects are expected to broaden the power deposition. Too high hydrogen minority concentration, derived from visible spectroscopy, could also contribute to this low electron heating with ICRH. It should be noted that the global confinement compared to the ITER96-L scaling law (H96-L) is reduced by only ~7% when ICRH is added suggesting an efficient ion heating.

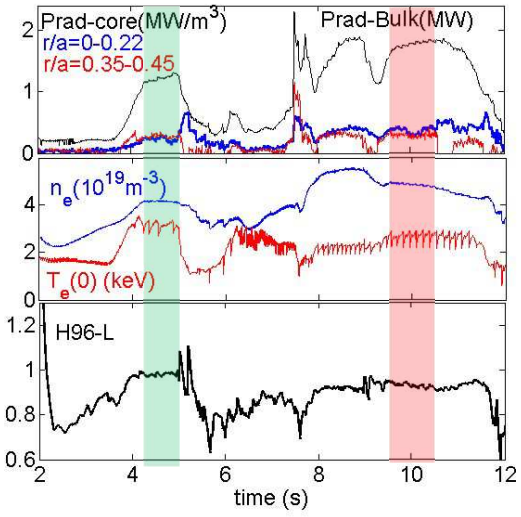

Figure 11. Discharge 55568 with a 3MW LHCD-only phase (green shaded) and a LHCD+ICRH phase (2MW+3MW, red shaded)

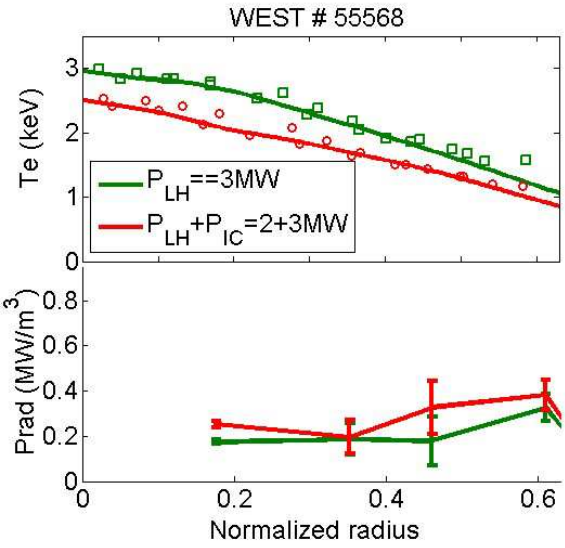

Figure 12. Electron temperature and radiation profiles of the discharge shown on figure 11. Electron density is 4.1 and $4.8\times10^{19}m^{-3}$ for the LH and LH+IC phase respectively.

5. Plasma radiation and core tungsten content

The high radiation capability of high Z elements such as W is a threat for maintaining a hot plasma with high energy confinement. Moreover, the neo-classical theory predicts an inward pinch of these impurities when the density and temperature profiles in the very core (r/a<0.3) are unfavorable. On WEST, since no NBI is used, the plasmas have a low toroidal rotation and are free of central particle source. Using GKW and NEO for the turbulent and neoclassical W transport respectively, we have found that the W neoclassical transport dominates over the turbulent one for r/a<0.25 [29]. Coherently W accumulation is generally not an operational issue on WEST. Only in a few discharges, the W asymmetry driven by ICRH could be the cause of an accumulation at low rotation [30]. However for core temperature in the range of 1-3keV, the W cooling factor which peaks for T_e=1.5keV is very unfavorable. As reported in section 3, by the existence of cold and hot electron temperature branches, for the development of the plasma scenarios, the interplay between the radiation and the electron heating of the bulk plasma was found to be an issue in the density and power ramp-up phase.

Over the C4 campaign database of all pulses with at least 1MW of RF power, the fraction of the total power which is radiated in the bulk of the plasma, $Frad_{Bulk}$, is ranging from 30% to 50% for most of the discharges (figure 13) [7]. On this large database, as expected from the discharge shown on figure 11, ICRH and LHCD heated plasmas exhibit similar fraction of radiated power (figure 13). Low fraction of radiated power occurs after boronization of the torus. $Frad_{Bulk}$ as low as 25% can be obtained with any combination of heating systems (LHCD, ICRH, LHCD+ICRH) as

shown on figure 14. The reduction of $Frad_{Bulk}$ lasts 1-10 pulses depending on the energy injected. Away from a boronization, the mean $Frad_{Bulk}$ value around 50% is not modified with an increasing RF power. $Frad_{Bulk}$ is also not density dependent at least up to $n_e = 4.5\times10^{19}m^{-3}$. In ohmic diverted plasmas, not shown on these two figures, this fraction is significantly higher: $Frad_{Bulk}$~65% far from boronization.

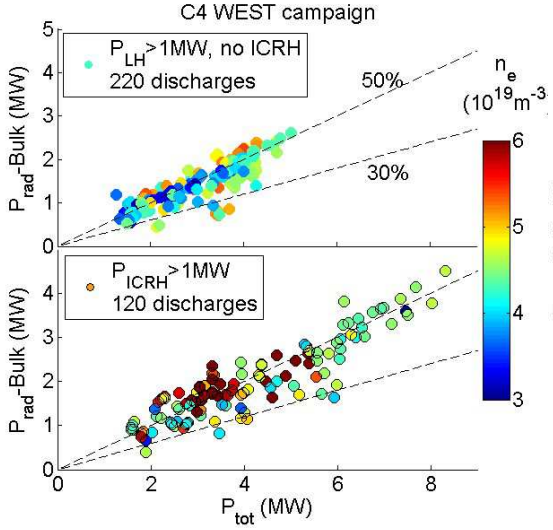

Figure 13. Prad-Bulk as a function of total power (Bt=3.7T, Ip=0.5MA). The color-bar denotes the line-averaged density of the plasma.

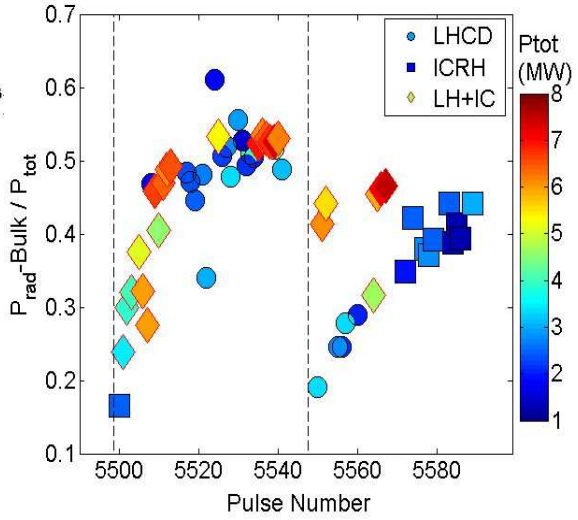

Figure 14. Time history of $Frad_{Bulk}$ *after two boronizations (dashed lines). The color-bar denotes the total power (Bt=3.7T, Ip=0.5MA).*

Mid-Z species could be expected to contribute to the radiation of the bulk. On WEST, the main mid-Z species sputtered from the main chamber is copper. The cooling factor of copper is 30 times lower than that of tungsten for a temperature of 3keV and reconstruction of the central soft X-ray and bolometry chords indicates that copper can be the main radiator at the plasma periphery (r/a>0.8) but does not contribute to the total bulk radiation by more than 20%.

In order to estimate the core W content, the 16 bolometry horizontal chords were inverted and, applying the cooling factors of W to the local value of radiation, and accounting for the measured ECE T_e profile, a 6-point profile of W density is obtained. The inversion is made up to T_e=1 keV, due to large uncertainties on the W cooling factor below such temperatures [31]. The estimated n_W is divided by the electron density (inversion from 10 interferometry chords). The W concentration in the core (r/a=0-0.22) is then plotted against the RF power. LHCD-only and ICRH-only pulses of C4 are compared in figure 15a and 15b respectively. There is no straightforward correlation between the fraction of radiated power and the ratio of n_W/n_e concentration in the core, as already reported when the line-averaged electron density was lower, mostly in the range of $3\text{-}4\times10^{19}m^{-3}$ [32].

Although the W concentration can be rather large at high power, up to 4×10^{-4}, there is no correlation between this concentration and the energy confinement. It should be noted that the OH phase of these discharges have similar core W concentration (figure 15-a), but lower W density as the electron density is lower by a factor 1.6 on average. A similar trend as for LHCD only pulses is observed for ICRH discharges (figure 15-b) as long as no W accumulation occurs. High plasma current (I_p=0.7MA) and density ($n_e>6.5\times10^{19}m^{-3}$) discharges have low core W concentration.

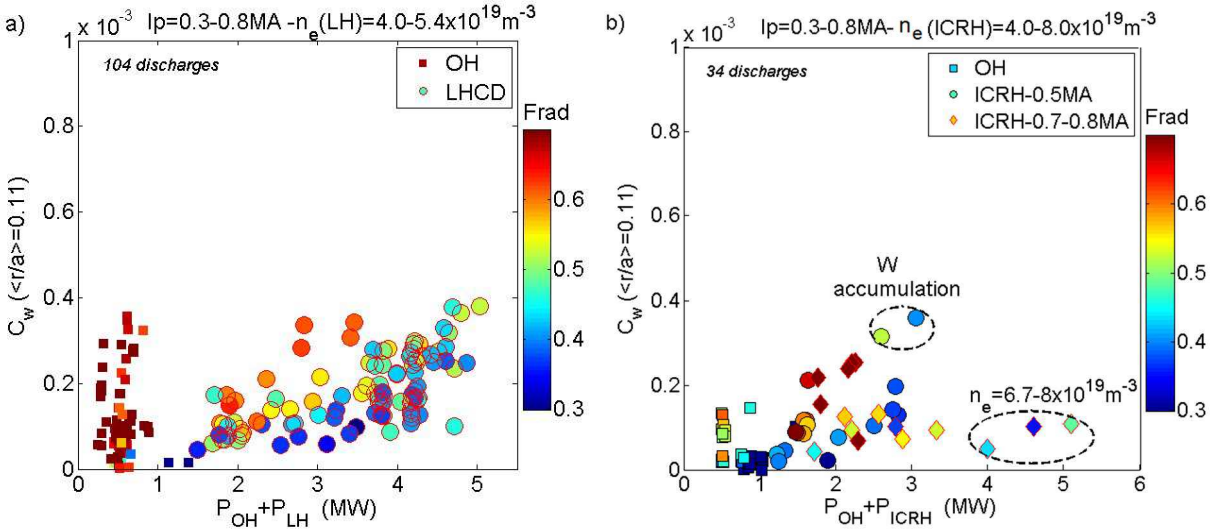

Figure 15. Core tungsten concentration of a) LHCD and b) ICRH discharges. The concentration of the ohmic heating phase is also shown (squares). Data are averaged on one-second time slice.

To compare more precisely W radiation and density of LH- and IC-heated C4 discharges (Ip=0.5-0.6MA), two databases were built with matched average power (1.6 MW) and line-averaged density ($4.8\times10^{19}m^{-3}$), one with LHCD only and the other with ICRH only. $Frad_{bulk}$ increases on average from 47% (LHCD) to 54% (ICRH) with a standard deviation of $\Delta Frad_{bulk}$=0.06-0.08, in line with values reported over a larger database (figure 13). For ICRH only pulses, the W densities in the core (r/a<0.4) are higher by almost a factor 2 but with no sign of peaking (figure 16-a). This is not inconsistent with an increase of the total radiation by only 15% as the core volume (r/a<0.4-0.5 with T_e>1keV) is only 20% of the total plasma volume. At higher power (3.7 MW) and higher density ($n_e=4.8x10^{19}m^{-3}$), 3 pulses can be compared: one LHCD-only and two LHCD/ICRH discharges. In this higher power range, in presence of ICRH, a more peaked central W density is reported (figure 16-b).

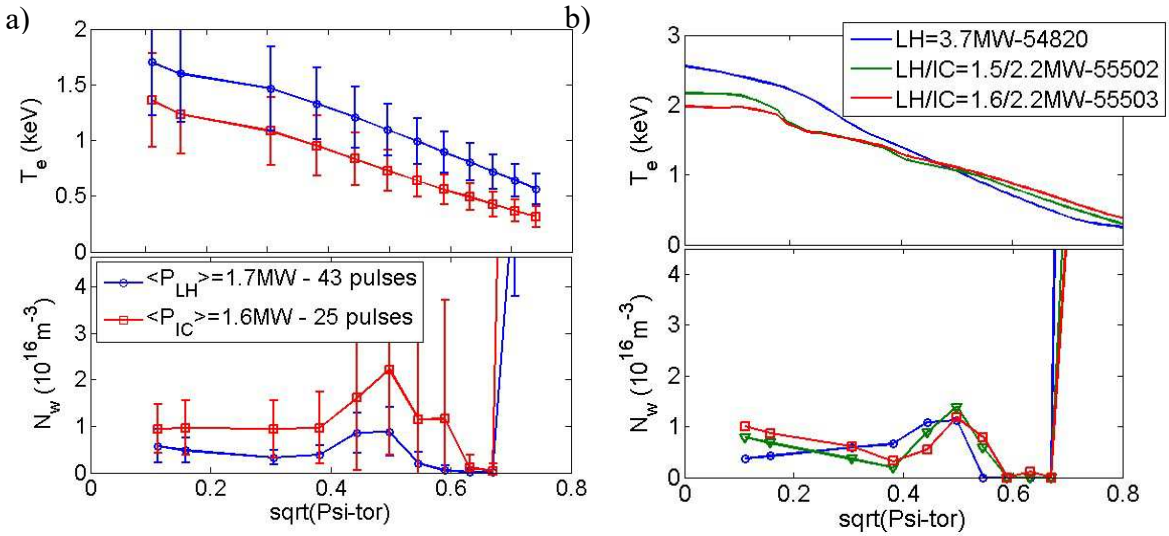

Figure 16. Electron temperature and tungsten profiles of a) LHCD and ICRH discharges, b) LHCD and LHCD/ICRH discharges with same total power. Tungsten densities at location where T_e is lower than 1keV are uncertain due to inaccurate knowledge of the cooling factor. Ip=0.5-0.6MA, $n_e=4.8\times10^{19}m^{-3}$. The standard deviation when averaging over the data set is indicated with a vertical bar.

6. Temperature collapse

During the high power phase, fast temperature collapse events could be observed in the different scenarios (IC, LH or LH+ICRH). In all cases, the collapse is initiated at the plasma centre by a local decrease of the electron temperature that progressively accelerates and often results in the triggering of MHD modes. Prior to this collapse, the radiation of the core starts increasing, typically 300ms before the central temperature collapse. Two examples of such collapses are shown in figures 17 (LH only) and 18 (LH and ICRH). Determining the precise description of how the event takes place requires a case to case analysis that is still on-going, but we can already identify the three main mechanisms at play: i) the W profile, ii) the electron heat source and iii) the core electron temperature. Regarding the first player, a peaking of the W profile is indeed inferred from the bolometry measurements in the plasma core (see fig. 17 and 18) after taking into account the cooling rate dependence on the temperature, as well as by UV spectroscopy measurements [33]. This peaking could be understood as the result of a neoclassical drive in ICRH discharges [30], or as a result of the initiation of the collapse itself, due to the loss of the ion temperature screening. The second player is the electron heat source. We have several indications that the radial profile of the LH deposition could be hollow, as supported by HXR measurements (see fig. 8) and by modelling [23, 34]. A depletion of the core heating could be reinforced as temperature decreases due to weaker absorption, leading to an unstable loop. The analysis of an LH heated pulse shows that these two first mechanisms need to be combined for reproducing the dynamics of a particular collapse [35]. For ICRH heating, the evaluation of the heat source involves the broadening of the deposition by finite orbit width effects, and a reduction by ripple losses or uncontrolled phase that remains to be quantified. When the correct ICRH antenna phasing is restored at t=7.65s, the core radiation strongly decreases and the temperature recovers above 3keV. Note that the two discharges of figure 18 have the same W antenna source following visible spectroscopy measurements. Finally, the core electron temperature contributes to the sensitivity of the discharge towards radiative collapse events, due to the bell shape of the W cooling rate between 1 and 3keV peaking at Te=1.5keV. Even if the W content would not vary, a reduction of the core temperature such as the one shown in figure 17 would result in an increased radiation. In this particular case of fig. 18, we have a decrease of the radiated power in the very core (r/a<0.11) as the temperature decreases, which indicates that the W content is decreasing even more in the core region as plasma density is increased. The sensitivity of LH deposition on the core temperature could therefore be an instrumental player in this particular case. Modelling of dynamics coupling the W cooling rates, the density increase, the LHCD absorption physics, the confinement modification is on-going using RAPTOR [36] and physics based transport models [35].

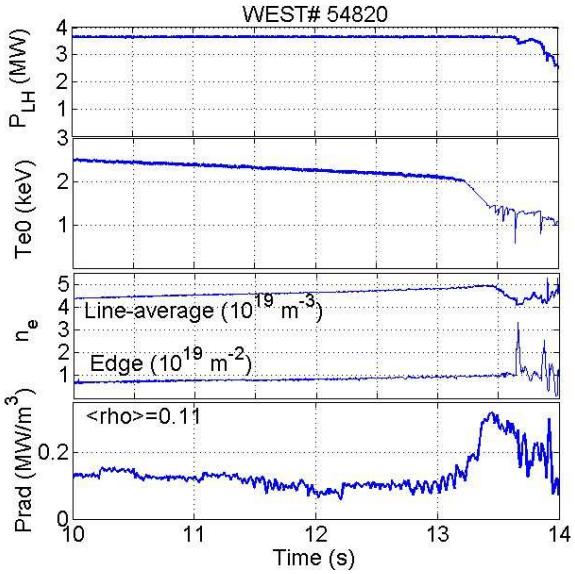

Figure 17. Thermal instability in a LHCD discharge. LHCD power is constant from t=5s

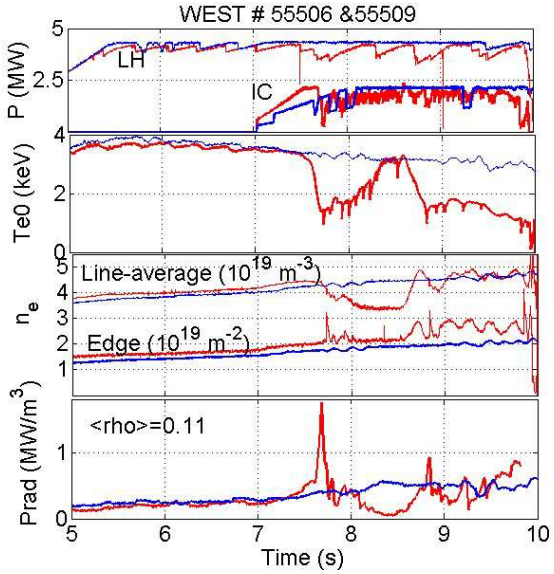

Figure 18. Thermal instability in a LHCD +ICRH discharge. One IC antenna of discharge 55506 (red lines) has an uncontrolled phasing between t=7.0s and t=7.6s.

7. Tungsten sources

In principle, the divertor W sources are strongly screened and the main chamber sources can be dominant for the core W contamination. Unlike in ASDEX Upgrade [37], the inner (high field side) wall is far from the separatrix on WEST (ΔR~20cm) (see figure 19) and cannot contribute significantly to the contamination. Concerning the RF antennas, they are all radially moveable and generally the three ICRH antennas are slightly closer to the plasma as compared to the two LHCD antennas (ΔR=5mm). The poloidal curvature of the plasma is such that the antennas are closer to the plasma by ~25mm above the mid-plane (z=+0.2m) compared to below the mid-plane (z=-0.2m) when operating in LSN as illustrated on figure 19.

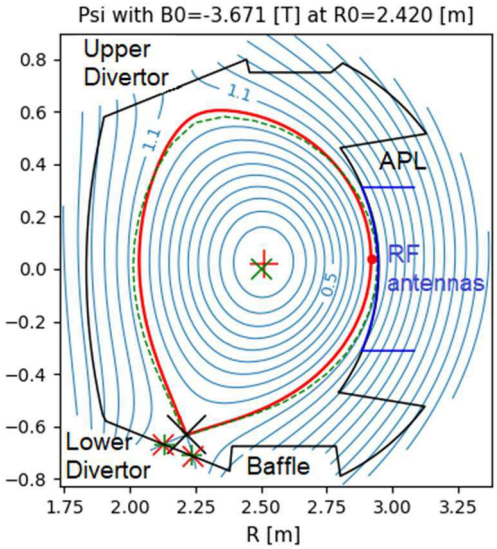

Figure 19: poloidal cut of a typical diverted WEST equilibrium in the vacuum chamber. The antenna protection limiter (APL) is moved backwards behind the antennas during the high power phase.

In addition to the W-coated guard limiters of the 5 RF antennas, the water-cooled upper divertor and the uncooled baffle near the lower divertor, both W-coated, are possible W sources. The baffle and the upper divertor are, respectively, quasi-aligned and 5-10 mm in front of the ICRH antennas. Moreover the length ΔR of the upper divertor which is in front of the RF antennas does not exceed 4-5cm indicating that these components are mostly in the shadow of the antennas and the protruding surface is close to the surface of the guard limiters framing the 5 antennas ($0.7m^2$). Therefore the eroded W flux from the upper divertor and baffle should not exceed that from the RF antennas by more than one order of magnitude. However modelling of the W transport from the emission at the wall to the confined plasma shows that the screening factor is at least two orders of magnitude larger for the upper divertor and baffle than for the antennas [38]. Taking advantage of the large gap (~15cm) between the confined plasma and the lower divertor in the USN configuration, the weight of these components in the LSN configuration on the total main chamber source can be experimentally estimated by comparing Prad-Bulk of discharges with same power, density and distance of the antennas to the separatrix (D_{ap}) for the two types of equilibrium. The comparison was done for several D_{ap} and Prad-Bulk was found systematically lower in the USN but the relative difference is estimated to be in the 0-15% range with high confidence. We conclude that these additional W sources should not contribute strongly to the plasma contamination and the main chamber sources are mostly originated from the antennas.
WEST W sources are estimated from a set of lines-of-sight of the visible spectroscopy diagnostic viewing the divertor plates (inner target and outer target) and the guard limiters of 3 antennas (LH1, LH2 and IC1 antennas) [39]. The photons flux of the neutral W line (λ=401nm) is converted in W atoms flux with the aid of the inverse of the photon efficiency S/XB [40]. The poloidal profile of the W emission of the WEST antenna protection limiter was successfully simulated with the coupled codes hPIC and RustBCA when these S/XB factors are used [41].
These heavy ions are prone to prompt redeposition and a model including the effect of the electric field is applied to calculate the fraction of atoms which are non-redeposited [42].

Both photon efficiency and prompt redeposition rate depend on local electron density and electron/ion temperature. These measurements are provided by a set of 16 (inner target) and 12 (outer target) Langmuir probes embedded in the tiles of the divertor inner target (IT) and outer target (OT) and by two reciprocating probes installed on the outboard limiter located slightly behind the RF antennas. For the LH and LH+IC experiments, the LH power reflections coefficient provides a good estimate of the density when this density lies between $1\times10^{17}m^{-3}$ and $1\times10^{18}m^{-3}$. For most of the discharges the maximum temperature on the divertor is in the 15-40eV range, the density is in the $2\text{-}7\times10^{19}m^{-3}$ range. Density and temperature near the antennas vary within a more limited range, $3\text{-}10\times10^{17}m^{-3}$ and 10-15eV respectively. The latter are less accurate, in particular in front of ICRH antenna as RF-induced convective cells develop causing unmeasured inhomogeneity of density. However when n_e and T_e are increased, S/XB and the prompt redeposition increase, and the net non-promptly redeposited W is finally found to be not very sensitive to the edge parameters in the vicinity of the antennas. Most of this non-promptly redeposited W flux $S_{w\text{-}non}$ will not cross the separatrix. We call SF_{MC} and SF_{div} (SF for 'screening factor'), the ratio of $S_{w\text{-}non}$ for the main chamber and divertor respectively to the W flux crossing the separatrix.

When 2MW of ICRH is added to a 4MW LHCD discharge, the main chamber sources that are monitored (right and left hand side limiters of LH1 and IC1, left hand side limiters of LH2 and outboard limiter APL) increase strongly by a factor 2.2 for LH antennas and 3.8 for the IC antenna whereas the lower divertor source increases very weakly, +10-20% for this discharge (figure 20). Also, one notes that the LH2 source is lower than that of the LH1 antenna: this source could be under-estimated as no line of sight views the right-hand side limiter of this antenna located 5mm behind LH1.

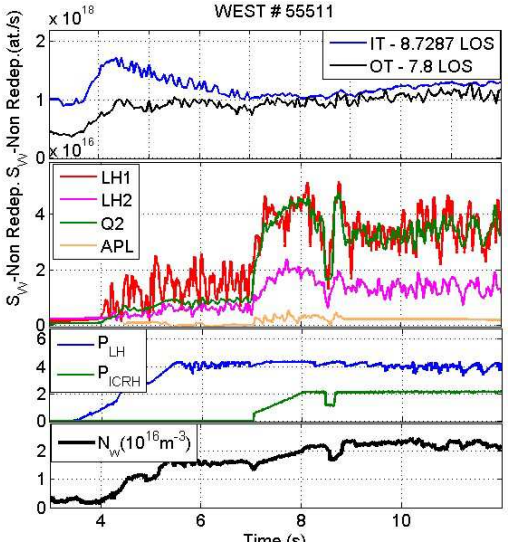

Figure 20 Non-prompt redeposited tungsten flux and tungsten density in the core (r/a<0.5).

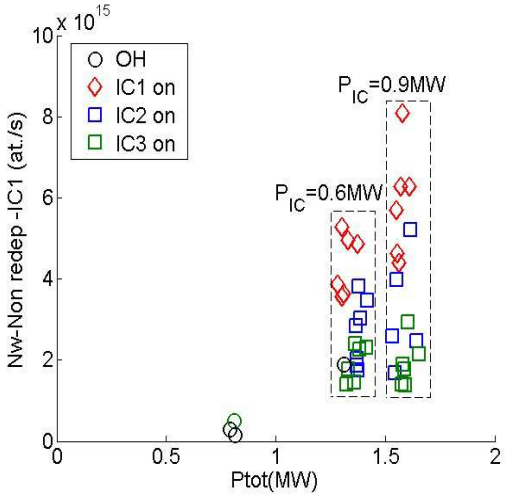

Figure 21. Non-prompt redeposited tungsten flux from IC1 antenna. Each IC antenna is powered alone.

The increase of W density in the core is estimated in the inner half of the plasma (deduced from bolometry for T_e>1keV) and is found to increase by +40%. Hence, for this case, we can conclude that the antenna sources contributes strongly but not exclusively to the W contamination of the core of the confined plasma.

Let us now focus on ICRH only heated plasmas, with either 0.6 or 0.9 MW of power. We can compare the level of non-redeposited W measured on the IC1 antenna limiter when: IC1 only is operated, the magnetically connected antenna IC2 only is operated and when the not connected antenna only is operated, namely IC3. The strong increase of the IC1 source, when this antenna is powered, is the result of the sputtering by ions accelerated in the RF sheath [43, 44]. As illustrated on figure 21, the non-redeposited W source on IC1 is amplified by a factor ~2 with P_{IC}=0.6MW and a factor ~3 with 0.9MW when comparing the situation with IC1 active to the case where IC3 non-magnetically connected is operated. Taking IC2 antenna, connected to IC1, as a reference, these amplification factors decrease to ~1.5 and ~2 respectively, confirming that RF sheath rectification on an active antenna could enhance the W erosion

on a passive magnetically connected object [45]. A strong increase of the antenna source is also observed when the antenna strap phasing is changed from 180° to 80° [46].
Unfortunately, the screening factors SF_{MC} and SF_{div} cannot be experimentally determined but the evolution of the penetration factor, when the RF input power increases, can be tracked by plotting the W density in the core as a function of the W sources.
In the following, the contribution of the non-monitored ICRH antennas (IC2 and IC3) is assumed to be equal to that of the IC1 antenna weighted by a factor $(P_{IC2}/P_{IC1})^{1/2}$ to take into account the scaling of the heat flux resulting from the RF sheath [47]. The same scaling was found for the plasma potential [48].
On figures 22 and 23, the W density in the core is plotted against the non-redeposited W sources measured on the various main chamber limiters (figure 22) and on the lower divertor inner and outer targets (figure 23). For both the main chamber and the divertor, at first the core W increases with the W sources until it saturates for larger sources. This could indicate that the screening factor increases and/or that the core W confinement is reduced as the sources increase.

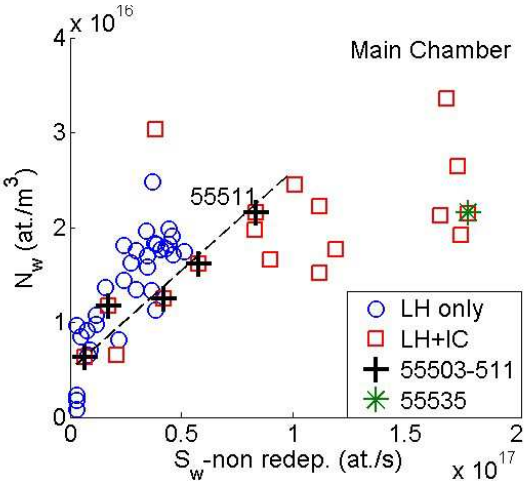

Figure 22. Tungsten density in the core plasma (r/a<0.5) versus estimated non-redeposited W sources of the main chamber.

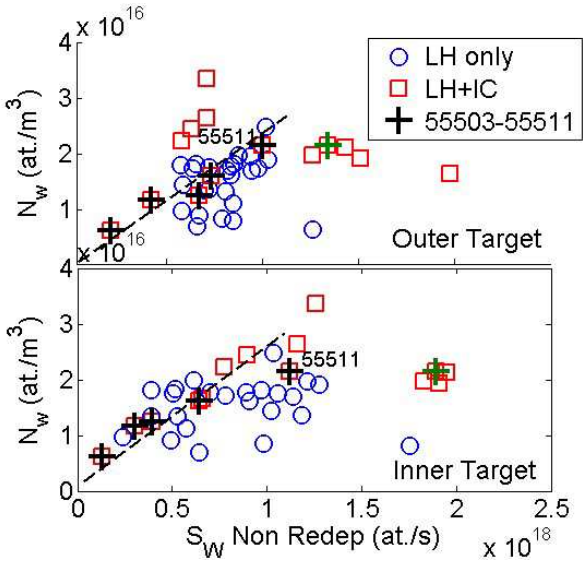

Figure 23 Tungsten density in the core plasma (r/a<0.5) versus estimated non-redeposited W sources of the divertor targets.

For a series of discharges performed the same day (#55503-55511, P_{LH}=1.6-4.3MW, P_{IC}=2MW), the W density scales almost linearly with divertor and main chamber sources indicating that neither the screening factors nor the W confinement time are changing from pulse to pulse (figures 22 and 23).
On the contrary, two discharges 55511 (black cross) and 55535 (green asterisk), performed on different days, with the same magnetic equilibrium, the same antennas positions are compared. The #55535 has more IC power (+0.7MW) and less LH power (-0.2MW). The W density is identical to #55511 despite a larger antenna source by a factor 2 and larger divertor sources by a factor 1.3 (outer target) and 1.6 (inner target).
Assuming N_w/τ_w to be a proxy for the W flux crossing the separatrix, the balance between the inward and outward fluxes can be expressed as:

$$N_w/\tau_w = S_{w\text{-non, MC}} / SF_{MC} + S_{w\text{-non, Div}} / SF_{div,} = S_{w\text{-non, MC}} / SF_{MC} + S_{w\text{-non, Div,IT}} / SF_{div,IT} + S_{w\text{-non, Div,OT}} / SF_{div,OT}$$

where $S_{w\text{-non, MC}}$ and $S_{w\text{-non, Div}}$ are the non-promptly redeposited fluxes from the main chamber and the divertor. Note that other W-coated objects not monitored, namely the baffle and upper divertor, could also contribute to the impurity contamination and would reduce the contribution of the divertor and the main chamber.
When the discharge has two high power phases (phase 1 and phase 2), the contribution of the main chamber to the plasma contamination, which reads $(S_{w\text{-non, MC}}/SF_{MC})/(N_w/\tau_w)$ is a function of 3 measured ratios and 1 unknown ratio:

$$MC\ contribution = \frac{\frac{N_{w,2}}{N_{w,1}} - \frac{\tau_{w,2}}{\tau_{w,1}}\frac{S_{w-no\ ,Div,2}}{S_{w-non,Div,1}}}{\frac{\tau_{w,2}}{\tau_{w,1}}\frac{S_{w-non,MC,2}}{S_{w-non,MC,1}} - \frac{N_{w,2}}{N_{w,1}}}$$

In order to fully determine the contribution of the main chamber, three assumptions need to be made:

- The screening factors do not change when the power is increased from phase 1 to phase 2. This should be the case when the plasma density is almost unchanged and the total power is increased by no more than 50%.
- The weight of the inner target on the total effective W source of the divertor for the plasma needs to be given. Following the modelling of a WEST discharge with very similar equilibrium, density, RF power [24], it was assumed that the inner target sources are much more screened than that of the outer target. In order to test the sensitivity of this assumption, the case when $SF_{IT}=SF_{OT}$ was also examined.
- The particle confinement time and the energy confinement time are decreasing with the same power scaling ($P^{-0.73}$), implying that $\tau_{w,2}/\tau_{w,1}$ would be reduced by about 30% for the two analyzed discharges. This parameter was varied between 0.5 and 1.0 for this analysis.

Manipulating only ratios of the same measured (W sources S_w and content N_w) or estimated (τ_w) quantity has the advantage to minimize the error as, for example, a systematic overestimate of a source by the same factor would cancel out.

This determination was made for the discharges 55511 and 55535 of figure 22 and 23 with the same high W contamination a shown in figure 24. The magnetic equilibrium and the line average density (n_e=4 and $4.2\times10^{19}m^{-3}$) are unchanged when going from phase 1 to phase 2. They both have 4 MW of LHCD in phase 1 and 6MW (#55511) and 7MW (#55535) of LHCD+ICRH power in phase 2. The contribution of the main chamber is estimated when the variation of the W confinement time $\tau_{w,2}/\tau_{w,1}$ is varied between 0.5 and 1. Plain circles highlight the case when the W confinement time scales like the energy confinement time. Assuming equal screening of these two sources would just slightly increase the MC contribution, for example from 0.65 to 0.7 when the 5 RF antennas are powered (discharge 55535). In case the upper divertor and baffle sources are not negligible, the MC source would be underestimated but assuming these additional sources increase the MC source by the same factor for the two time slices t1 and t2, the MC contribution is strictly unchanged and the RF antennas contribution is reduced. The upper divertor and baffle sources could increase less than antenna sources when the ICRH power is added to the LHCD power. It would result an increase of the MC contribution by typically 5% (for example from ~65% to ~70%) but contribution of the antennas would still be reduced.

The ratio SF_{IT}/SF_{MC} is also determined from the two particle balance equations. This ratio is found to be in the range of 7-15 when the inner target is fully screened. When including the prompt redeposition, which is more important on the divertor targets than on the antennas (lower density), this ratio is in the range of 20-50.

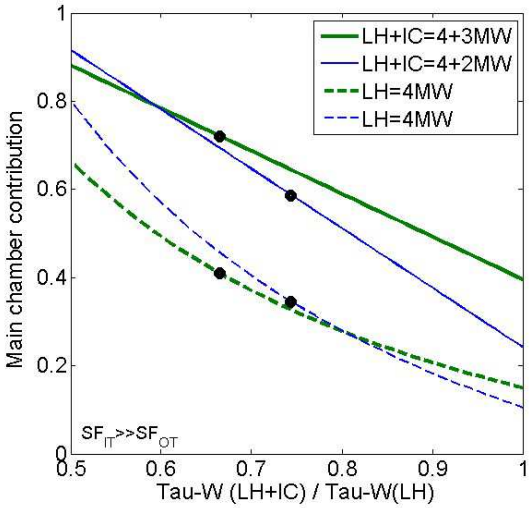

Figure 24. Main chamber contribution to the total tungsten content of the confined plasma as a function of $\tau_{w,LH+IC}/\tau_{w,LH}$ *for discharges 55511 (blue lines) and 55535 (green lines). Plain circles highlight the case when* $\tau_{w,2}/\tau_{w,1} = \tau_{E,2}/\tau_{E,1}$

8 Conclusion

High RF power experiments combining LHCD and ICRH have been conducted on the full W WEST tokamak up to 9.2 MW. Two types of pulses are obtained, some in which Te0 increases with increasing P_{tot}/n_e as expected, and some where the plasma does not burn-through W radiation and Te0 remains below 2keV even with increasing P_{tot}/n_e. The RF power and density ramps need to be well adjusted for access to high confinement plasmas.

On the hot branch, good performance L-mode plasmas with high electron temperature and high confinement (following the ITER L96 scaling) in stationary conditions are achieved despite 50% fraction of radiated power in the bulk plasma. Thanks to more than additional 1000 WEST entries in the ITER L mode database, at aspect ratio A ranging from 5 to 6, the weak impact of A on the L mode confinement is confirmed. Energy confinement is very weakly dependent on the density up to $4.5\times10^{19}m^{-3}$.

H-mode has been accessed, lasting up to 4s. But the increment in total energy is mild despite the formation of a pedestal. This improved confinement regime has been obtained so far only at a power exceeding marginally the threshold, and with oscillatory phases due to increasing radiation once the pedestal density forms.

In ICRH and LHCD heated plasmas, the radiated power, due to W, is similar and high ($Frad_{Bulk}$ ~50%). It can be decreased for 1 to 10 pulses down to 25% after boronization of the walls. The RF antennas can be a major contributor to the W content in the plasma bulk. With the 5 antennas coupling 7 MW to the plasma, the contribution of the main chamber could reach up to 70% of the total sources. However the W density in the core does not increase as fast as the W sources thanks either to an enhanced screening factor or, more likely, to a reduced core W confinement.

In WEST phase 2, the ICRH power will be further ramped up with better control of the minority species in order to maximize the central electron heating which should be favorable in particular to burn through W. The H mode access will be explored at higher density and higher power. From the LHCD efficiency achieved in H-mode, very long pulses (t>100s) at high density ($\geq 5\times10^{19}m^{-3}$) could be achieved with 6MW of LHCD with more bootstrap current.

Acknowledgements

This work has been carried out within the framework of the EUROfusion Consortium and the French Research Federation for Fusion Studies and has received funding from the Euratom research and training programme 2014-2018 and 2019-2020 under grant agreement No 633053. The views and opinions expressed herein do not necessarily reflect those of the European Commission.

Appendix. Details of scaling law

To highlight the level of correlation between the regression parameters, the correlation matrix is reported in table 2.

Table 2 – correlation matrix for WEST database merged with ITER database.

	I_p	B_{tor}	P_{tot}	n_e	k	R	M	A
I_p	1	-	-	-	-	-	-	-
B_{tor}	0.32	1	-	-	-	-	-	-
P_{tot}	0.74	0.45	1	-	-	-	-	-
n_e	0.12	0.30	0.17	1	-	-	-	-
k	-0.04	-0.10	-0.18	0.19	1	-	-	-
R	0.45	0.48	0.52	-0.26	-0.08	1	-	-
M	-0.12	0.15	-0.21	0.12	0.33	0.07	1	-
A	-0.77	0.16	-0.45	0.03	0.17	0.05	0.26	1

As expected, there is a general correlation between plasma current, heating power and aspect ratio. In general, larger machines operate at higher currents and therefore higher heating power. The correlation between plasma current and aspect ratio is the result of the $B_{tor}/(I_p.A)$ dependence of the safety factor q which does not vary by more than a factor 2 for most of the discharges.

The analysis taking the radiated power into account is shown in the table 3. The power used to evaluate the energy confinement time and the regression coefficient is computed as P_{tot}-$P_{rad,bulk}$.

Table 3 – dimensional and dimensionless scaling laws for WEST database (line 1), ITER database (line 2 and 4 and WEST database merged with ITER database (line 3 and 5).

	I_p	n_e	P_{tot}-$P_{rad,bulk}$	A	B_T	k	R	M_{eff}	Ent.
τ_{th} ITER-L scaling	0.96	0.40	-0.73	0.06	0.03	0.64	1.83	0.20	1313
ITER + WEST data	1.01	0.26	-0.76	0.15	0.18	0.63	168	0.22	2396
	q	B_T	k	A	M_{eff}	ρ_*	ν_*	β	Ent.
τ_{th} ITER-L scaling	-3.74	0	3.22	0.04	0.67	-1.85	-0.19	-1.41	1313
ITER +. WEST data	-4.30	0	3.67	0.01	0.73	-1.62	-0.09	-2.18	2396

References

[1] Pütterich T et al 2013 Plasma Phys. Control. Fusion 55 124036
[2] Casson F 2015 Plasma Phys. Control. Fusion 57 014031
[3] Bourdelle C. et al., Nucl. Fusion **55**, 063017 (2015)
[4] Nardon E. et al., Magnetic configuration and plasma start-up in the WEST tokamak', 45th EPS Conference on Plasma Physics, 2018, Prague, Czech Republic
[5] Ph. Moreau et al., IEEE Transactions on Plasma Science, Vol.48, No.6, June 2020, pp 1376-1381
[6] Liang A.S. et al, «optimization of LH wave coupling for the WEST LHCD launchers», this conference
[7] Hillairet J. et al, Nucl. Fusion 61 (2021) 096030, https://iopscience.iop.org/article/10.1088/1741-4326/ac1759/pdf
[8] Bucalossi J. and the WEST team, «Operating a full tungsten actively cooled tokamak: overview of WEST first phase of operation», Nucl.Fusion 2021 https://iopscience.iop.org/article/10.1088/1741-4326/ac2525/pdf
[9] Gaspar.J et al, 2021 Nucl. Fusion 61 096027
[10] Kaye S.M. and ITER Confinement Database working Group 1997 Nucl. Fusion 37 1657
[11] Faugeras, B. 2020. «An overview of the numerical methods for tokamak plasma equilibrium computation implemented in the NICE code». Fusion Engineering and Design 160, 112020.

[12] Luce T.C. et al. , Plasma Phys. Control. Fusion, 50, (2008) 043001 (87pp)
[13] Maslov M. et al 2020 Nucl. Fusion 60 036007, https://iopscience.iop.org/article/10.1088/1741-4326/ab6482/pdf
[14] Sarazin Y. et al, .2020 Nucl. Fusion 60 016010
[15] Hoang T. et al., 2014 Nucl.Fusion **34** pp 75-85
[16] Loarer T. et al 2020 Nucl. Fusion 60 126046
[17] Martin Y.R. et al., Journal of Physics: Conference Series 123 (2008) 012033
[18] Vermare L. et al., «Formation of the radial electric field profile in WEST tokamak», this conference
[19] Ryter F., et al Nucl. Fusion **54** (2014) 083003
[20] Solano E. et al, FEC2021
https://conferences.iaea.org/event/214/contributions/17057/attachments/10157/14796/IAEA_2021_Solano_Proc_v7.pdf
[21] Solano E. et al., "Power balance analysis at the L to H transition in JET-ILW", 23rd Joint EU-US Transport Task Force Meeting, Seville, 2018
[22] Goniche M. et al., Physics of Plasmas **21** 061515 (2014)
[23] Peysson Y.et al., «Effect of partially ionized high-Z atoms on fast electron dynamics in tokamak plasma», this conference
[24] Lau C. et al, «Lower hybrid electric field magnitude and polarization measurement and modeling results on the WEST tokamak», APS DPP 2021
[25] Martin E.H. et al., (2019), 59(7), 076006.
[26] Maget et al., submitted to PPCF
[27] Artaud J.F. et al., Nucl. Fusion 58 (2018) 105001 (25pp)
[28] Dumont R.J., Nucl. Fusion 49 (2009) 075033 (14pp),
[29] Yang X. et al., Nucl. Fusion 60 (2020) 086012 https://iopscience.iop.org/article/10.1088/1741-4326/ab9669/meta
[30] Maget P. et al, «Collisional transport and poloidal asymmetry distribution of impurities in tokamak plasmas», , TH/P728.
[31] Pütterich T. et al 2019 Nucl. Fusion 59 056013
[32] Goniche M. et al., AIP Conference Proceedings **2254**, 030002 (2020); https://doi.org/10.1063/5.0014034
[33] Guirlet R. et al., 2nd IAEA Meeting of the Global Network for the Atomic and Molecular Physics of Plasmas, 6-10 December 2021
[34] Wallace G.M et al., 47th EPS Conference on Plasma Physics, http://ocs.ciemat.es/EPS2021PAP/pdf/P4.1047.pdf
[35] Ostuni V. et al., TTF 2021 York
[36] F. Felici et al, Nucl. Fusion, 51(8):083052, (2011)
[37] Dux R et al., Journal of Nuclear Materials 390–391 (2009) 858–863
[38] Di Genova S.et al., 2021 Nucl. Fusion 61 106019
[39] Meyer O. et al., Rev. Sci. Instrum. 89, 10D105 (2018), https://doi.org/10.1063/1.5035566
[40] Johnson C., Auburn University, private communication
[41] Klepper, C.C., 47th EPS Conference on Plasma Physics, submitted to PPCF.
[42] Chankin A.V., Coster D.P. and Dux R., -Plasma Phys. Control. Fusion 56 (2014) 025003 (11pp)
[43] Urbanczyk G. et al. Nucl. Fusion 61 (2021) 086027 (19pp), https://doi.org/10.1088/1741-4326/ac0d11
[44] Colas L. et al. « First Application of Ion Cyclotron Resonant Frequency Waves on WEST Plasma Scenarios »,
[45] Urbanczyk G. et al. «Metallic impurity content behavior during ICRH-heated L-mode discharges in EAST», Nucl. Fusion 60 (2020) 126003 (19pp) https://doi.org/10.1088/1741-4326/abae82
[46] Hillairet J. et al., Nuclear Fusion 2021 https://iopscience.iop.org/article/10.1088/1741-4326/ac1759/pdf
AIP Conference Proceedings 2254, 040004 (2020); https://doi.org/10.1063/5.0013571
[47] Colas.L et al., « Key results of long pulse ICRH operation in Tore Supra », Nucl. Fusion, 46, S500 (2006). doi:10.1088/0029-5515/46/7/S11
[48] Wukitch S.J., « ICRF specific impurity sources and plasma sheaths in Alcator C-Mod », Journal of Nuclear Materials 390–391 (2009) pp.951–954, doi:10.1016/j.jnucmat.2009.01.245